2023 FINESST Progress Report: Infrared Stellar Occultation Studies of Saturn's Atmosphere from Cassini VIMS

An

March 14, 2023

Abstract

I started grad school in Fall 2016. I settled on an advisor and began scoping out and understanding this project in the Fall of 2018. In the Spring of 2019, I applied for and was awarded this grant over the Summer. I began work in the Fall of 2019. During that time, I created a preliminary analysis of the imaging-mode occultations as a launchpad for the rest of the analysis. In January of 2020, I put the grant on hiatus to help an emergency management start up. The grant resumed in 20 August 2022. I have been reacquainting myself with the field of astronomy, my skills in physics, and my previous work. This progress report represents my analysis of the work that I did during this grant's previous active period, my plans to complete the promised analysis of the Cassini VIMS occultation data per my proposal, a discussion of planned publications using these data to constrain models of Saturn's atmospheric chemistry, applications to understanding photochemistry in exoplanet atmospheres, applications to brown dwarf atmospheres, applications to astrobiology, applications to Uranus, and applications to Titan research.

1 Administrative

Title of Grant: Stellar Occultation Studies of Saturn's Atmosphere
Type of Report: Progress Report
Name of the principal investigator: Philip Nicholson
Period Covered by the report: 2022-08-20 to 2023-03-15
Cornell University, 418 Space Sciences Building, Ithaca, NY 14853
Grant Number: 80NSSC19K1528

2 Data Analysis: Objectives and Accomplishments

Cassini VIMS observed over 100 occultations by Saturn of background stars, a handful of which were observed through a series of small-frame images instead of a single spatial

pixel pointed at the star's initial location on the sky. These imaging-mode occultations provide a chance to directly observe the stars' refraction through the outer layers of Saturn's atmosphere and constrain the relative importance of differential refraction to other sources of attenuation in the photometry of an occultation. This is an important calibration for the higher-radial-resolution occultation-mode data, for which the image of the star much more quickly gets refracted out of the field of view.

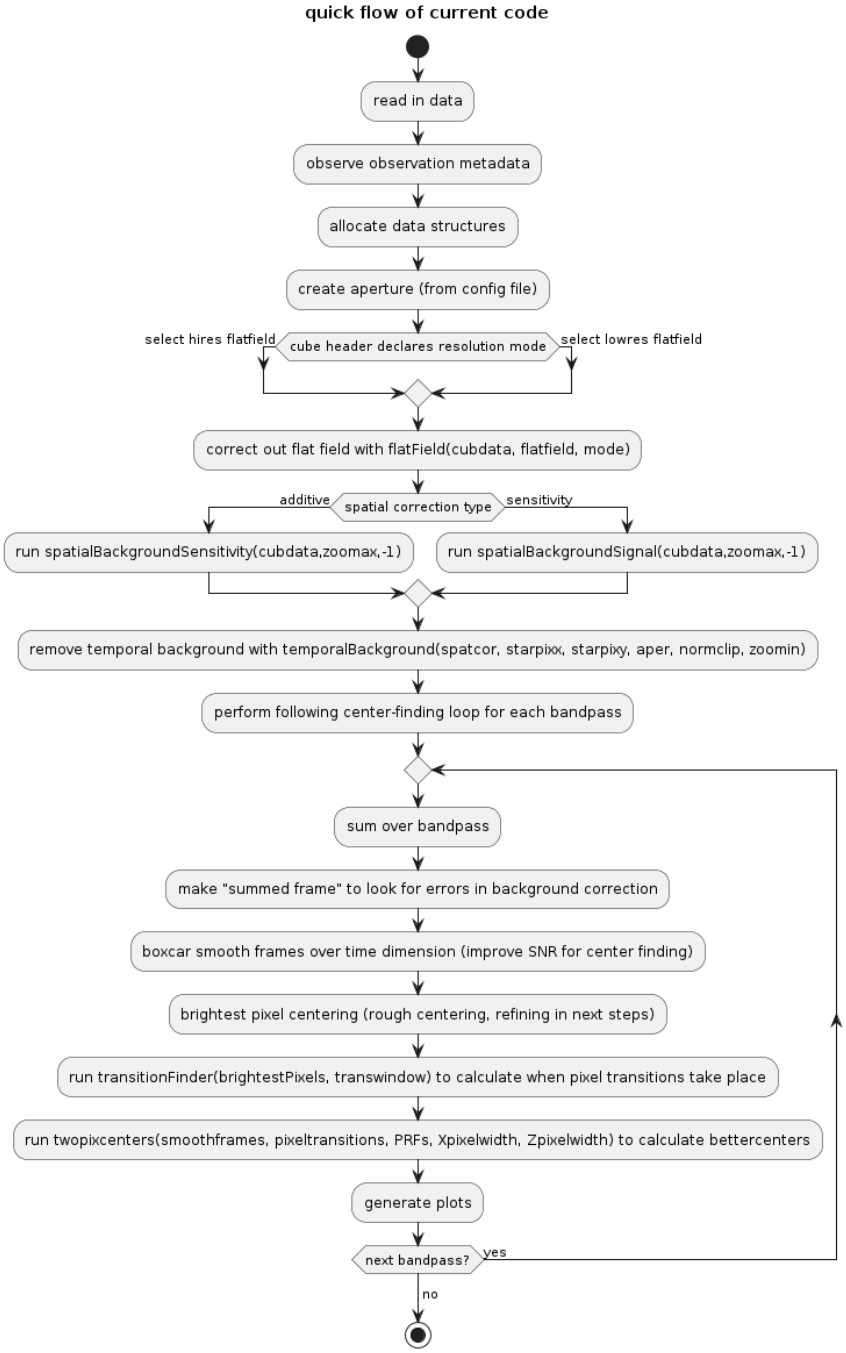

Figure 1: code flowchart for current version

As such, my initial analysis targeted these imaging-mode occultations. I wrote a code that looks like Figure 1. It corrects out known sources of noise and performs standard aperture photometery. It produces lightcurves, X and Z centering results to track the star getting refracted out of frame, differences in the star's center by wavelength, spectra, and movies of these properties during the event, an example can be seen in Figure 2

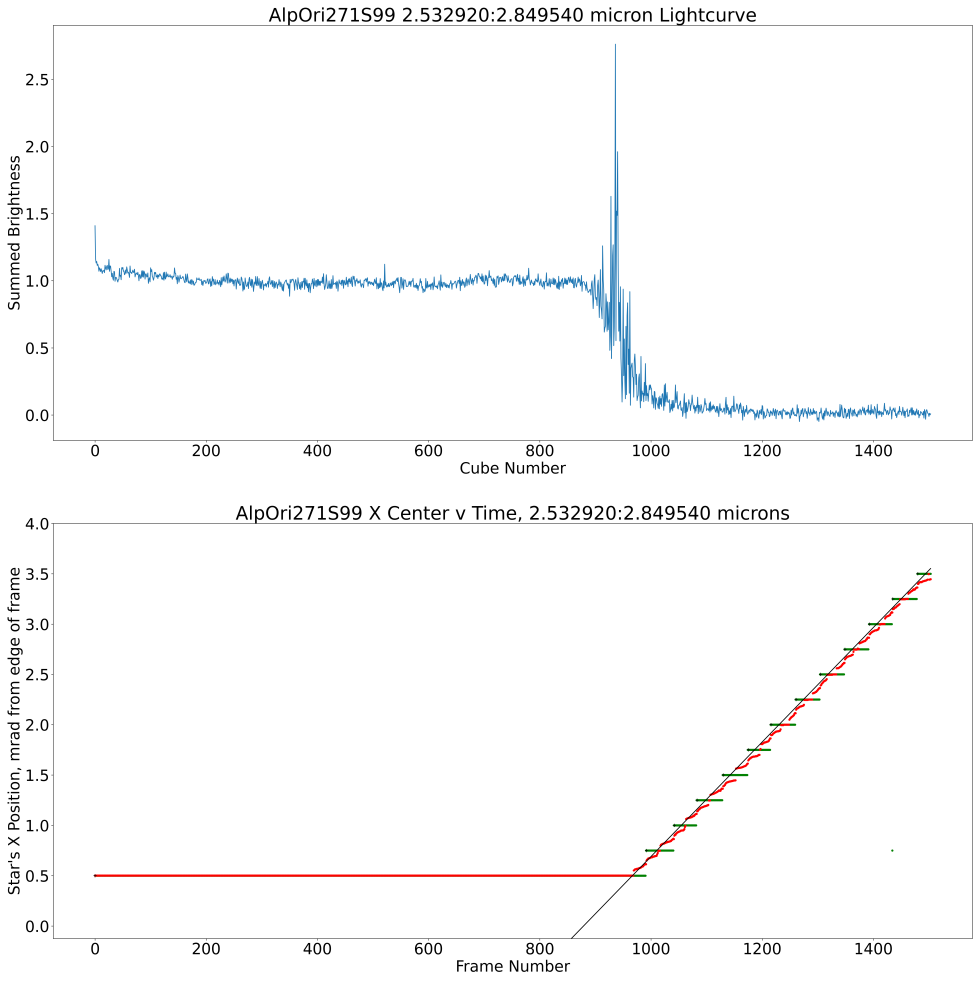

Figure 2: Lightcurve and centering results for an occultation of AlpOri (Betelgeuse) on orbit 271, observed in the 2.7 μm continuum band. The top plot displays the flux dropping and twinkling through the atmosphere. The bottom plot displays the centroid location calculated for the star, plotted over a line with a slope matching the spacecraft's velocity. This is one of four types of plots produced by the code. See the code outline document for more details.

There are four major tasks of the code. Two of them have been implemented in some

form, and are iterating towards completion. These two act on only the imaging-mode data. The two tasks remaining to write act on all data.

2.1 Background Subtraction

The standard aperture photometry methods employed are insufficient for these data. There isn't always a "sky", and the background level changes as the limb of the planet enters and then engulfs the field of view. A more honest background correction needs to model this moving limb of the planet as having a different background flux for each frame's background correction. Discussions on implementing this have begun. Detail on the current implementation can be found in the code outline document. For now, we are not yet ready to describe the new background correction in detail.

2.2 Centering Algorithm

See the Centering document for a full discussion.

Tracking the center of a star in a VIMS image is a difficult task because the PSF of the star is less than one pixel. Still, the star is rarely centered in a pixel, and so centering can be achieved by looking at how much light spills into the neighbors of the brightest pixel. Fortunately, the Pixel Response Function (PRF) is well-defined for the single VIMS spatial pixel as a function of the angle between the center of the pixel and the star. This has been done by slewing the spacecraft so that the star AlpOri (Betelgeuse) raster-scans across the pixel. From these, we can calculate the theoretical relative brightnesses of the pixels on either side of the brightest pixel relative to the brightest pixel, and compare this to the measured value in the VIMS frame.

First, we must determine which two pixels share the most starlight. To do so, we:

1. integrate over a continuum bandpass to improve signal to noise (e.g. 2.53-2.85 microns)
2. perform a boxcar smoothing in time (usually 10 frames)
3. record the brightest pixel for each resulting timestep
4. locate "transition times" when the brightest pixel changes from one timestep to the next
5. at each timestep select the brightest pixel and the brightest pixel on the other side of the nearest "transition"

We measure the direction to the star by taking the ratio (R_{data}) of the de-noised signal in these two selected pixels. We compare this ratio to the same ratio calculated from the PRF scans $R_{scans}(t)$ at each time step t. We calculate the value of $t = t_0$ for which $\chi^2 = (R_{data} - R_{scans}(t_0))^2$ is minimized, and then calculate $\theta(t_0)$ which is the offset of the star from the center of the pixel at t_0.

$$R^x_{data} = \frac{P^{x\pm1}}{P^x} \tag{1}$$

And in the z direction this ratio is defined as:

$$R^z_{data} = \frac{P^{z\pm1}}{P^z} \tag{2}$$

Where $P^x = P^z$ is the brightness of the brightest pixel (integrated over some wavelength range), and $P^{x\pm1}$ and $P^{z\pm1}$ are those of the adjacent pixels in each direction.

This metric has many properties which make it useful. Theoretically, it should be monotonically increasing or decreasing as the star position increases steadily in pixel position. For PSFs smaller than a pixel, there will be a plateau at zero where there is no light observed in the neighboring pixel. Away from this plateau (near the pixel boundaries) we have the best sensitivity to the position of the star. At metric values $R = 1$ the center of the star's PSF straddles the boundary with the neighboring pixel and we have the most sensitivity.

The current version of the code performs fits in each direction independently, and using manually-selected PRF scan track numbers. A planned improvement is to fit both simultaneously, which will allow the algorithm to self-select the best track for each direction.

After this step, we have occultation profiles in the same form as the occultation-mode data. This ends the imaging-mode specific portion of the code. The following two subsections describe code that will be run on all occultation data.

2.3 Calculating Temperature and Pressure from Refraction in the Continuum Bands

The current version of the code does not yet perform this calculation.

Consider a light ray from the occulted star incident on a spherical planet of radius R, at an impact parameter ρ. As it penetrates more deeply into the atmosphere, where the refractive index of the gas is larger, the ray gradually refracts towards the planet's center until it reaches a minimum radius, after which it traces a mirror-image path back out of the atmosphere.

The formal expression for the overall angular deflection of the ray once it emerges from the atmosphere is:

$$\theta(\rho) = -2\rho \int_{r_0}^{\infty} \frac{dn/dr}{n\sqrt{n^2r^2 - \rho^2}}\, dr, \tag{3}$$

where $n(r)$ is the refractive index profile of the atmosphere, and the ray's minimum radius r_0 is specified by the condition $n(r_0)r_0 = \rho$.

Adjacent light rays are deflected by progressively larger amounts as ρ decreases and the rays penetrate more deeply into the atmosphere. As a result of this *differential refraction*, the flux of light from the source is reduced by a factor of Φ:

$$\Phi(\rho) = \left(1 - D\frac{d\theta}{d\rho}\right)^{-1} \left(1 - \frac{D\theta}{\rho}\right)^{-1}, \tag{4}$$

where D is the distance from the planet to the observer. The second factor represents the focusing effect that occurs near the center of the geometric shadow and can be neglected for our data where $D\theta \ll \rho$.

As described in Elliot et al. (1977) and French et al. (1978), we can use these two expressions to perform an inverse Abel transform and invert our occultation lightcurves in regions of the spectra dominated by differential refraction to acquire multiple **radial profiles of the temperature and pressure in the planet's stratosphere.**

This technique is standard for inversions of differential-refraction dominated stellar occultations. Due to Saturn's highly oblate shape, the above expressions are adjusted in practice to use a local spherical fit to the atmosphere.

We are confident that the attenuation of the starlight at wavelengths where hydrocarbon molecular absorption is negligible is dominated by the above-described impact of differential refraction and not aerosol-driven scattering extinction. Although aerosols are an important chemical component of Saturn's atmosphere, these particles are likely sub-micron in size and their scattering efficiency should decrease rapidly with decreasing wavelength, perhaps scaling as λ^{-q} where q is between 1 and 4. The aerosols on Titan follow such a power law with $q \simeq 1.8 \pm 0.5$ (Bellucci et al., 2009). The extinction in the VIMS Saturn occultations at wavelengths outside of the strong hydrocarbon bands is observed to be essentially *independent* of wavelength, strongly suggesting that aerosol extinction is negligible at the few mbar level and above and therefore we may neglect them in our models. **One goal of the imaging-mode occultations is to test this assumption by following the star much deeper into the occultation than is available in occultation-mode, and directly measuring the bending angle (distance the image has moved across the detector) and the flux to compare to values predicted by the above equations.**

2.4 Calculating Molecular Abundances from Spectra

The current version of the code does not yet perform this calculation.

Let's consider an "onion-skin" model of an atmosphere for which each thin radial layer is of uniform composition and density. As a ray of star light passes through each of these layers, it is attenuated according to the equation:

$$\Phi(\lambda) = \Phi_0 \; e^{-\delta\tau(\lambda)}, \tag{5}$$

where Φ_0 is the attenuation experienced before entering that layer and $\delta\tau(\lambda)$ is the optical depth of the layer as a function of wavelength, described by the equation:

$$\delta\tau(\lambda) = \kappa(\lambda) L d \tag{6}$$

Here, κ is the absorption coefficient, L is the slant pathlength, and d is the density of the layer which is known from the inversion of the lightcurve at the refraction-dominated continuum wavelengths.

The data for a given occultation can be thought of as a time-series of spectra, each of which cuts a deeper path through the atmosphere than its predecessor. Each time-step can be used to constrain the opacity of an additional deeper layer, and then be used as an input to the next timestep since that layer will also be probed during the subsequent observations. Datapoints can be binned in time to increase signal to noise at the expense of the radial resolution of the resulting abundance profile. We call this technique "onion-peeling" and a

preliminary proof-of-concept using a single wavelength bin was presented by Banfield et al. (2011).

We will fit a model to a full-spectrum $\kappa(\lambda)$ calculated in each layer from our data. A model spectrum will be calculated with a line-by-line approach using Voigt profiles calculated using the pressures and temperatures from our refraction inversions described above. We will use line list databases such as the HITEMP database from HITRAN [1] (Gordon et al., 2017) for each gas relevant to Saturn's atmosphere. The contributions of each gas (chiefly CH_4 and C_2H_6, but possibly also C_2H_2) to the final opacity are independent and proportional to their mixing ratios, which will be fit to the data.

In practice, hydrogen and helium are essentially transparent in the near-infrared for any reasonable path length through the stratosphere [2] so the opacity is dominated by trace gases, methane, ethane, and acetylene (Moses and Greathouse, 2005).

3 Status Changes and Budget

Should I request travel funding to DPS or the Uranus workshop?

4 Results to Eventually Disseminate

I need help to flesh these out. I will use these bullets as a starting point to help me find committee members.

- Overview of Cassini occultation data analysis
- Seasonal variations of photochemistry. This effect is visible by eye, and should be quantifiable with our data.
  - Comparison to (Fletcher et al., 2010) CIRS observations where CH4 distribution could not be uniquely determined from CIRS alone. See if we can help break that degeneracy?
  - Comparison to (Moses and Greathouse, 2005) and (Fouchet et al., 2009) 1-D chemistry models
  - Tying these models to the canonical D.F. Strobel 1969 paper on the "methane cycle", and updating that framing
  - Comparison to predictions from various exoplanet atmospheric models that are currently "in vogue"? How well do these models fit the atmosphere of an endo-planet? Should we test them directly while peeling the onion?
  - Comparison to what we know about / expect to find in Uranus???
- Paper on the chemistry of aerosols produced at the end-stage of photochemistry

[1] https://hitran.org/hitemp

[2] H_2 does have a fundamental vibrational transition at 2.1 μm, which is detectable in the spectra of the Jovian planets, but this is a collision-induced absorption that scales as p^2, and so is very weak in the stratosphere, even for very long path lengths.

- sedimentation, nucleation, cloud-seeding (Fletcher et al., 2018)
- astrobiological implications?
- What can we say about complex organics sedimenting down into a region of convective ammonia cloud condensation? What kinds of amino-organic compounds might they form?
- compare to titan chemistry?

What originally got me interested in this project was the relationship to photochemistry models in exoplanet atmospheres. The astrobiological implications have kept me interested in this topic, and helped to guide me back to the relative safety of grad school when I was far from anything familiar. Titan is also very lovely and I want to apply what we learn on Saturn to constrain Titan's similar photochemical processes. Brown dwarves are also kind of like big giant planets, and might also be an interesting avenue of comparison... if they even have photochemistry? Dick French collected all of the historical Uranus occultation experiments on PDS (French et al., 2023). This is a future dataset to which this code and analysis can be applied.

References

Banfield, D., Gierasch, P. J., Conrath, B. J., Nicholson, P. D., Hedman, M. M. 2011. Saturn's He and CH4 Abundances from Cassini VIMS Occultations & CIRS Limb Spectra. EPSC-DPS Joint Meeting 2011 1548.

Bellucci, A., Sicardy, B., Drossart, P., Rannou, P., Nicholson, P. D., Hedman, M., Baines, K. H., Burrati, B. 2009. Titan solar occultation observed by Cassini/VIMS: Gas absorption and constraints on aerosol composition. Icarus 201, 198-216.

Elliot, J. L., French, R. G., Dunham, E., Gierasch, P. J., Veverka, J., Church, C., Sagan, C. 1977. Occultation of Epsilon Geminorum by Mars. II - The structure and extinction of the Martian upper atmosphere. The Astrophysical Journal 217, 661-679.

Fletcher, Leigh and Achterberg, Richard and Greathouse, Thomas and Orton, Glenn and Conrath, B. and Simon, Amy and Teanby, Nicholas and Guerlet, Sandrine and Irwin, P. and Flasar, F. 2010. Seasonal change on Saturn from Cassini/CIRS observations, 2004-2009. Icarus 208, 337-352.

Fletcher, L. N. Greathouse, T. K. Guerlet, S. Moses, J. I. West, R. A. 2018 Saturn's Seasonally Changing Atmosphere Saturn in the 21st Century, 251-294.

French, R. G., Elliot, J. L., Gierasch, P. J. 1978. Analysis of stellar occultation data - Effects of photon noise and initial conditions. Icarus 33, 186-202.

Richard G. French and Colleen A. McGhee-French and Mitchell Gordon and Richard L. Baron and Amanda S. Bosh and Marc W. Buie and Nancy Chanover and Mary Ann Clark and Edward W. Dunham and Linda M. French and Ian S. Glass and Jay D. Goguen

and Brooke Gregory and Rachel A. Hock and Julie A. Kangas and Stephen E. Levine and Keith Y. Matthews and Emily C. McMason and Karen J. Meech and Jessica Mink and Philip D. Nicholson and Michael J. Person and Françoise Roques and Bruno Sicardy and Bringfried Stecklum and David Tholen and Eliot F. Young and Leslie A. Young. 2023. Uranus Ring Occultation Observations: 1977-2006. Icarus 395, 0019-1035.

Fouchet, T. and Moses, J. I. and Conrath, B. J. 2009. Saturn: Composition and Chemistry Saturn from Cassini-Huygens, 83-112.

Gordon, I. E. Rothman, L. S. Hill, C. 2017. The HITRAN2016 Molecular Spectroscopic Database Journal of Quantitative Spectroscopy and Radiative Transfer 203, 3-69.

Moses, J. I., Greathouse, T. K. 2005. Latitudinal and seasonal models of stratospheric photochemistry on Saturn: Comparison with infrared data from IRTF/TEXES. Journal of Geophysical Research (Planets) 110, E09007.